Thermochemical stability of silicon–oxygen–carbon alloy thin films: A model system for chemical and structural relaxation at SiC–SiO_2 interfaces

D. M. Wolfe, B. J. Hinds, F. Wang, G. Lucovsky,[a] B. L. Ward, M. Xu, R. J. Nemanich, and D. M. Maher
Departments of Materials Science and Engineering, Physics, and Electrical and Computer Engineering, North Carolina State University, Raleigh, North Carolina 27695-7907

(Received 1 February 1999; accepted 29 March 1999)

Alloy thin films of hydrogenated silicon–oxygen–carbon $(Si,C)O_x$ $x<2$, were deposited and analyzed in terms of changes in structure and bonding as a function of rapid thermal annealing between 600 and 1100 °C using a combination of Fourier transform infrared spectroscopy, Raman scattering and high-resolution transmission electron microscopy. Results showed that three structural/chemical transformations took place upon annealing. The initial reaction (600–800 °C) involved the loss of hydrogen bonded to both silicon and carbon. At intermediate temperatures (900–1000 °C) a Si–O–C type bond was observed to form, and subsequently disappear after annealing to 1050 °C. The formation of ordered amorphous-SiC regions, nanocrystalline-Si regions, and stoichiometric, thermally relaxed SiO_2 accompanied the disappearance of the Si–O–C bond at the 1050 °C annealing temperature. Using this alloy as a model system, important information is obtained for optimized processing of SiC–SiO_2 interfaces for device applications. © *1999 American Vacuum Society.* [S0734-2101(99)16104-9]

I. INTRODUCTION

The attainment of a low defect density gate oxide on SiC substrates is critically important in optimizing the electrical performance of field effect transistor devices. In particular, the interface between the substrate and the gate oxide plays a key role in determining transistor performance characteristics and reliability.

Considering first the Si–SiO_2 interfaces, studies based on x-ray photoelectron spectroscopy (XPS) of Si–SiO_2 interfaces prior to postoxidation annealing have identified an interfacial compositional transition layer within 0.5 nm of the interface which contains intermediate oxidation states of Si, i.e., Si^{1+}, Si^{2+}, and Si^{3+} or suboxide (SiO_x, $x<2$).[1–3] This transition region can contribute to interface roughness and also give rise to electronically active defects. Improvement of device properties is typically achieved following a postoxidation anneal.[4] Analysis of interface bonding chemistry and structure has shown that the improvements after annealing derive from reductions of suboxide bonding groups in interfacial transition regions, effectively smoothing the Si–SiO_2 interface.[4–13]

Studies of SiC–SiO_2 interfaces have also identified an interfacial compositional transition layer.[14–16] Depending on the substrate polytype, oxidation temperature, and ambient (wet versus dry), results have shown that carbon atoms may become trapped in the growing oxide as they outdiffuse from the interface, forming an oxycarbide interface layer. For example, Hornetz, Michel, and Halbritter have shown[14] using angle resolved XPS that a thin layer (1 nm) with an approximate composition $Si_4O_2C_{4-x}(x<2)$exists at the SiC–SiO_2 interface, and that graphite may be present on the top surface of the oxide. Using Auger electron spectroscopy (AES) Chaudhry[15] reported carbon contents in wet oxides grown on 3C–SiC as high as 14%, and that dry oxides contained much more silicon than stoichiometric SiO_2, i.e., suboxide character, indicating that wet and dry oxidation differ in mechanism considerably for 3C–SiC. The effect of carbon in the oxide and the reported nonstoichiometric suboxide on the electrical performance of SiC metal–oxide–semiconductor field effect transistor devices is unknown. Transistor characteristics following various postoxidation annealing treatments have been reported by Lipkin and Palmour,[17] with improvements being noted in interface trap density and electron mobility. The effect of this postoxidation anneal, however, is not well understood microscopically. Therefore, a fundamental understanding of the bonding environment when carbon is incorporated into the oxide and its effect on suboxide formation is needed, especially in light of (i) the numerous substrate polytypes, (ii) the speculation regarding oxidation mechanisms,[18] and (iii) room temperature channel electron mobility values which are substantially lower than those measured in the bulk.[17]

This article extends studies of the thermal stability of plasma-deposited SiO_x thin films[19–21] to suboxides of Si and C, $(Si,C)O_x$. The research identifies changes in structure and bonding using Fourier transform infrared spectroscopy (FTIR), Raman scattering, and high-resolution transmission electron microscopy (TEM), as a function of rapid thermal annealing (RTA) temperatures that are of importance for understanding changes in interface bonding and chemistry occurring during the thermal oxidation of SiC and subsequent annealing of the SiC–SiO_2 interfaces. In particular, a Si–O–C type bonding group is identified to form in the films between 900 and 1000 °C annealing temperature, and subsequently disappear at 1050 °C. The results of this research

[a]Electronic mail: gerry_lucovsky@ncsu.edu

then provide important information under pinning SiC device processing technology.

II. EXPERIMENT

Thin films of hydrogenated $(Si,C)O_x$ approximately 200 nm in thickness were deposited on fused quartz and high resistivity (15 Ω cm) *p*-type Si wafers in an ultrahigh vacuum (UHV) multichamber system using a remote plasma enhanced chemical vapor deposition (RPECVD) process, as described elsewhere.[22] The fused quartz substrates were used for Raman studies to eliminate spectral interference from a crystalline-Si substrate peak. For FTIR analysis, high resistivity Si wafers were used to minimize free-carrier absorption in the substrate. The wafers were also single side polished and ''orange peel'' roughened on the other side to minimize multiple reflections in the substrate and reduce background interference fringes.

Prior to sample insertion into the load lock of the deposition system, (i) a 15 s HF dip (50:1) followed by (ii) a 1 min deionized water rinse and (iii) nitrogen blow dry were performed on the Si wafers. A 10 min ultrasonic bath in a sulfuric/chromic acid glass cleaning solution followed by (i) a 10 min deionized water rinse and (ii) a nitrogen blow dry was done on the fused quartz. Films of $(Si,C)O_x$ were deposited at 250 °C and 300 mTorr using (i) excited species (e.g., O_2^* and O atoms) transported out of an upstream He/O_2 radio frequency plasma, and (ii) neutral species from downstream injected SiH_4/CH_4 mixtures.[23] Alloy compositions for the films were determined by XPS and Rutherford backscattering (RBS). The composition of the $(Si,C)O_x$ films was; $x \sim 0.15$ and C$\sim$10 at. %, with an uncertainty of ±0.02 at. %. For baseline reference and comparison, thin films of hydrogenated SiO_x, $x \sim 0.15$ and SiC_x, $x \sim 0.2$, were also prepared by similar RPECVD processes. The local bonding environments and structure in these three different types of alloy films was studied using a combination of FTIR, Raman, and high-resolution TEM, as a function of RTA temperatures between 600 and 1100 °C. Characterization was performed before and after direct annealing to the desired temperature at a ramp rate of 100 °C/s in 1 atm Ar for 90 s. For FTIR analysis, spectra were subtracted from a reference Si wafer. An Ar^+ laser operating at 514.53 nm, with incident laser power on the sample of approximately 150 mW, was used for Raman scattering analysis. High-resolution TEM imaging was performed on cross-sectional samples, prepared using standard cutting and polishing techniques, in the bright-field mode with an accelerating voltage of 250 kV.

III. EXPERIMENTAL RESULTS

A. SiO_x baseline

Figure 1 shows FTIR absorption spectra before and after annealing to various temperatures for SiO_x ($x \sim 0.15$) thin films. Three distinct spectral features are noted and shift upon annealing. The peak of 630 cm^{-1} is a Si–H bending mode[24] and is a result of hydrogen incorporation (~15 at. %) into the growing film from the source gas SiH_4. Upon an-

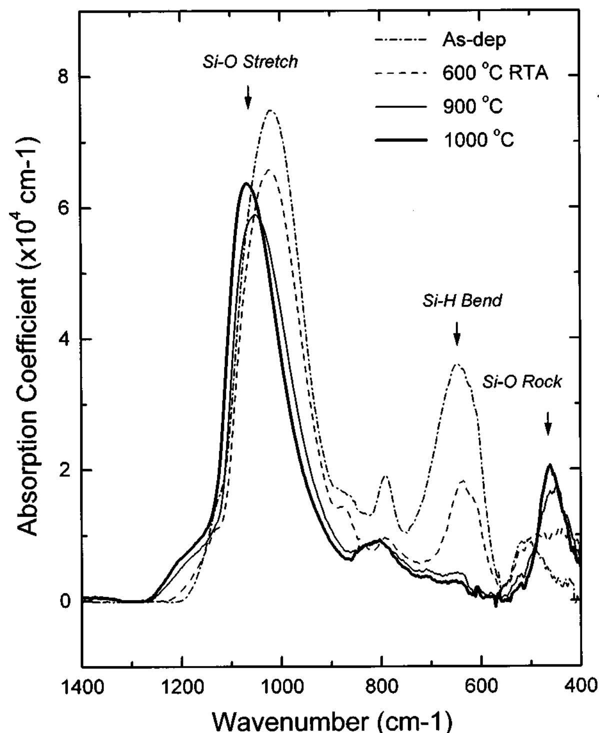

FIG. 1. FTIR absorption spectra of SiO_x, ($x \sim 0.15$) thin films before and after annealing.

nealing to temperatures greater than about 800 °C this feature completely disappears, demonstrating the initial reaction upon annealing to temperatures of about 600 °C involves the loss of bonded hydrogen to silicon from the films. The decrease in the infrared peak at 630 cm^{-1} is accompanied by a similar decrease in a coupled Si–O–Si–H vibration at 780 cm^{-1}.[24] Once hydrogen is lost, this feature is replaced by a Si–O bond bending mode at ~810 cm^{-1}. The intense peak in between 1015–1080 cm^{-1} is the Si–O bond stretching mode.[24] In the as-deposited films, this Si–O stretching mode is located at ~1017 cm^{-1}, indicative of suboxide bonding arrangements.[6,19,24] As the annealing temperature is increased the Si–O stretching mode shifts towards higher frequencies, signifying that atomic rearrangement is occurring and that suboxide bonding is being reduced. This feature becomes characteristic of stoichiometric and thermally relaxed SiO_2 (Refs. 6,13) after annealing to approximately 900 °C. The third distinguishing Si–O feature is the Si–O bond rocking mode located at ~440 cm^{-1}. This mode becomes pronounced after annealing to approximately 900 °C, and again is characteristic of stoichiometric and thermally relaxed SiO_2.

Figure 2 shows Raman spectra of SiO_x, $x \sim 0.15$ thin films before and after annealing to various temperatures. The spectra for the as-deposited films indicated that they were amorphous and were not compositionally homogeneous. A transverse acoustic phonon mode at 150 cm^{-1} was observed, indicating that amorphous-Si (*a*-Si) regions were present. The onset of nanocrystalline-Si (*nc*-Si) formation in the films was observed in the spectra by the emergence of an optical

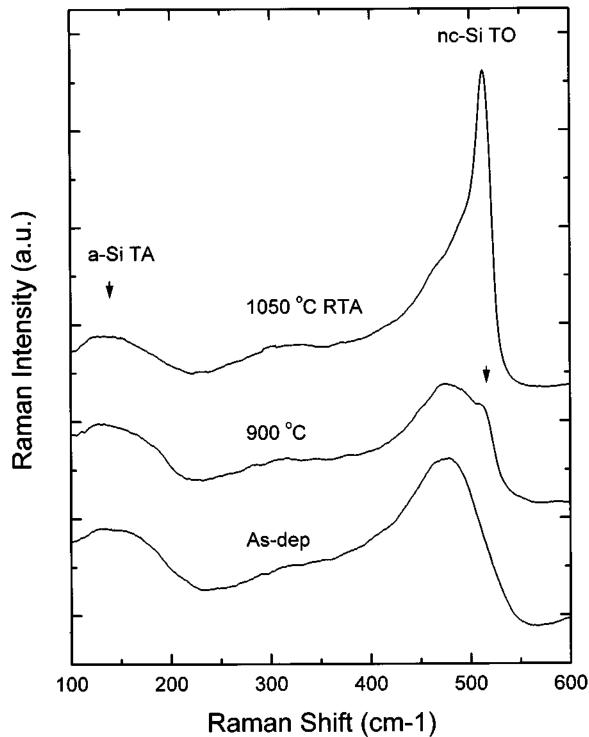

FIG. 2. Raman scattering spectra of SiO_x, ($x\sim0.15$) thin films before and after annealing.

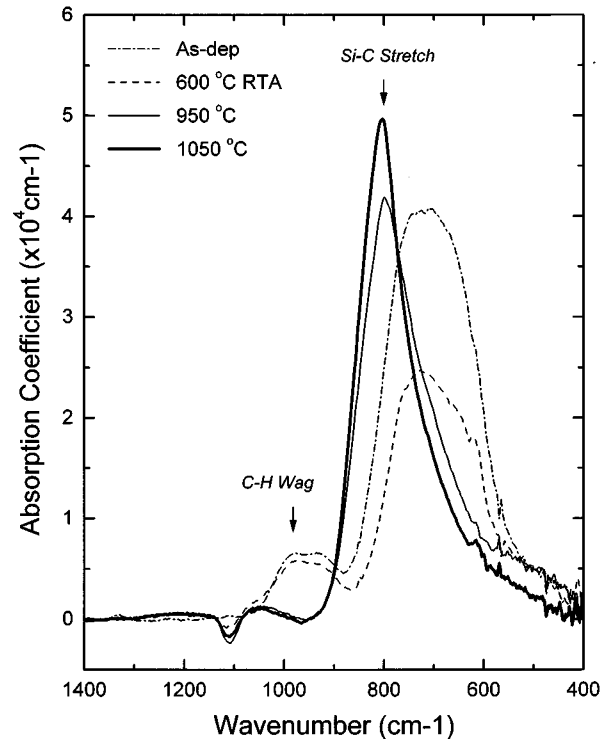

FIG. 4. FTIR absorption spectra of SiC_x, ($x\sim0.2$) thin films before and after annealing.

phonon mode at 515 cm^{-1}. In Fig. 2, this feature is just becoming observable after annealing at 900 °C and is clearly pronounced after annealing to 1050 °C.

Consistent with Raman analysis, Fig. 3 shows a digitally enhanced, high-resolution TEM image of a SiO_x film, $x\sim0.15$ after annealing to 900 °C. Randomly oriented Si crystallites, as verified through selective area diffraction, were observed to form through out the films, with their size increasing as the annealing temperature was increased. The size of the crystallites that formed after annealing to 900 °C was approximately 10 nm. The box in Fig. 3 outlines a typical Si crystallite.

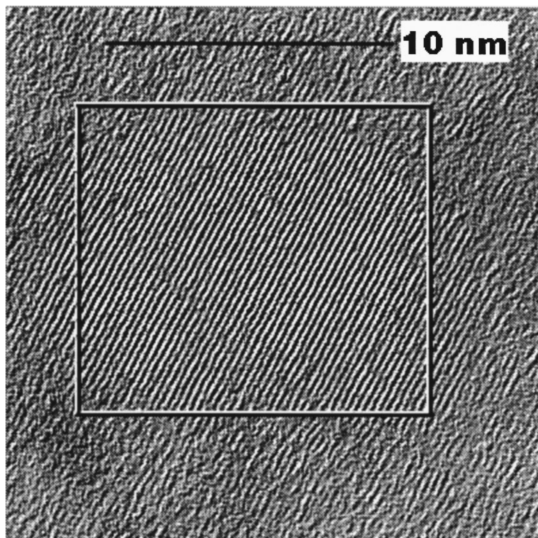

FIG. 3. High-resolution TEM image of a SiO_x,($x\sim0.15$) thin film after annealing to 900 °C.

In summary, the significant bonding and morphology changes that occur between as-deposited films and films annealed at 900 °C correspond to the formation of stoichiometric and structurally relaxed SiO_2 regions (from FTIR analysis) and nanocrystalline-Si regions (from Raman and TEM analysis).

B. SiC_x baseline

Figure 4 shows FTIR spectra before and after rapid thermal annealing to various temperatures for SiC_x thin films, $x\sim0.2$. Analysis of the spectra shows that the initial reaction involves the loss of hydrogen bonded to silicon and carbon. The modes between 900 and 1000 cm^{-1} are due to C–H bond wagging motions[25] and disappear above 700 °C annealing temperature. The intensity of the Si–H bending mode at 630 cm^{-1}drops sharply after annealing above 800 °C. A Si–CH bond wagging mode,[25] which is present in the same vicinity as the Si–H bending mode, and very weak Si–CH bond bending mode[25] present at about 1340 cm^{-1} both decrease upon annealing to about 800 °C. Most evident in the spectra is the appearance of a relatively narrow Si–C bond stretching mode located at 800 cm^{-1} after annealing to 950 °C. Further increases in annealing temperature shift this mode towards higher frequencies, indicating increased C to Si coordination.[26]

Figure 5 shows Raman spectra before and after annealing to various temperatures for SiC_x thin films, $x\sim0.2$. The as-

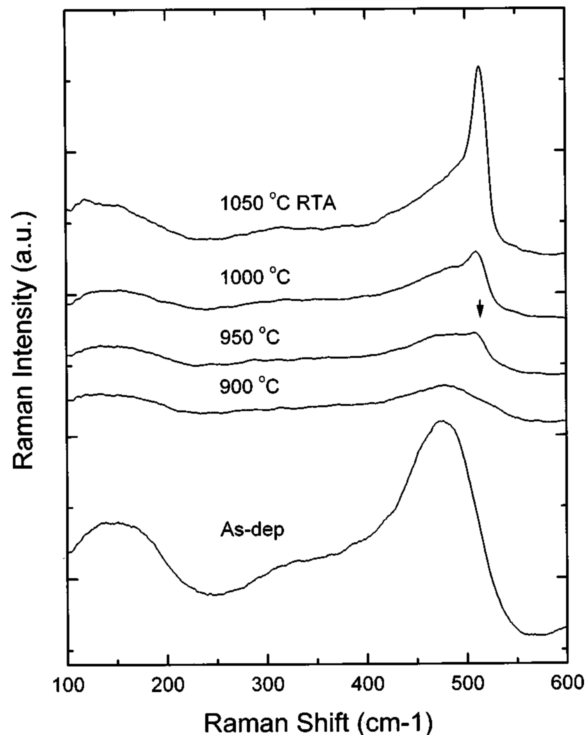

FIG. 5. Raman scattering spectra of SiC_x, ($x\sim0.2$) thin films before and after annealing.

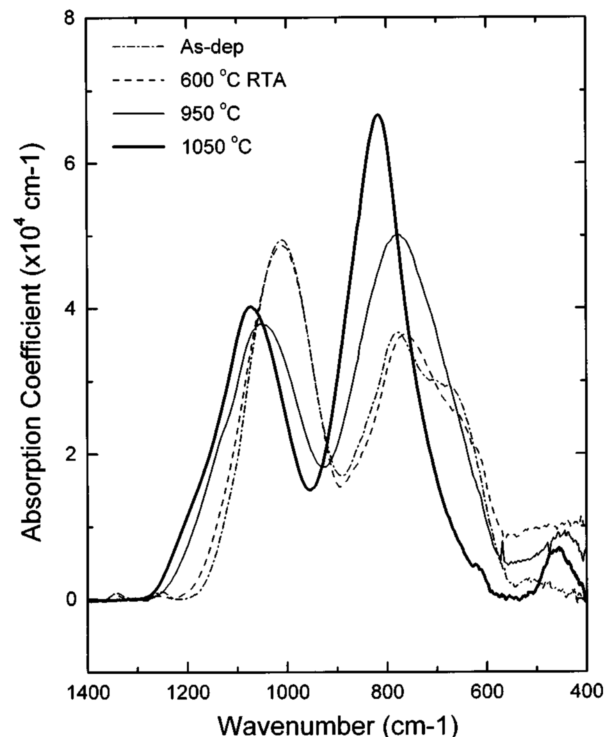

FIG. 6. FTIR absorption spectra of $(Si,C)O_x$, ($x\sim0.15$ and C$\sim$10 at. %) thin films before and after annealing.

deposited films were amorphous and compositionally inhomogeneous, as similarly shown for the SiO_x films above. Also, as in the case for the SiO_x films, Raman spectra of the SiC_x films show that Si crystallization occurs after high temperature annealing. As shown in Fig. 5, the feature at 515 cm^{-1} represents the formation of nanocrystalline-Si regions, and occurs after annealing to approximately 950 °C. Note that no other phonon modes of any other crystalline phases such as SiC were observed. For example, for all of the crystalline SiC polytypes, both the transverse and longitudinal optical phonon[27] modes occur at between 780 and 980 cm^{-1} and were not detected. Also, neither crystalline nor amorphous carbon–carbon vibrations were detected. High-resolution TEM imaging (not shown) is consistent with these results, and in particular, no crystalline phases other than silicon were observed in the selective area diffraction patterns.

In summary, the significant bonding and morphology changes that occur between as-deposited films and films annealed at 950 °C correspond to the formation of chemically ordered *a*-SiC regions (from FTIR analysis) and nanocrystalline-Si regions (from Raman and TEM analysis).

C. $(Si,C)O_x$

After establishing baseline reference results for SiO_x and SiC_x films, results are now presented for films in which CH_4 has been added to the Si suboxide source gas mix of SiH_4 and O_2 to form $(Si,C)O_x$ alloys. Figure 6 shows FTIR spectra before and after annealing of $(Si,C)O_x$ films, $x\sim0.15$ and C$\sim$10 at. %. As shown in Fig. 6, the spectra are essentially a combination of the SiO_x and SiC_x spectra, however, with several important and subtle differences. For these films, the initial thermally driven annealing reaction also involved the loss of bonded hydrogen from both Si–H and C–H groups, as explained above for SiC_x films. A well defined Si–C bond stretching mode located at 800 cm^{-1} emerges in the $(Si,C)O_x$ spectra, but after annealing to 1050 °C rather than 950 °C, as for the SiC_x films. Further increases in annealing temperature again shift this mode towards higher frequencies, indicating increased C to Si coordination.[26] Similar to the SiO_x films, in the as-deposited $(Si,C)O_x$ films, the Si–O stretching mode is initially located at 1015 cm^{-1}, indicative of suboxide bonding arrangements. As the annealing temperature is increased the Si–O stretch mode shifts towards higher frequencies, signifying that atomic rearrangement is occurring and that suboxide bonding is being reduced. However, at approximately 900 °C a shoulder located at $\sim$1125 cm^{-1} is observed to form on the high frequency side of the Si–O stretch mode, and is attributed to Si–O–C bonding groups[25,28,29] on the basis of its frequency relative to the Si–O–Si stretch mode. In the Si–O–C bonding group, oxygen is the bridging atom between $Si–O_4$ and $O–Si–C_3$ tetrahedra. This feature is not observed after annealing to 1050 °C, and stoichiometric, thermally relaxed SiO_2 is formed. The implications of this added feature in the spectra will be addressed in Sec. IV.

Figure 7 shows Raman spectra before and after annealing of (Si,C,O_x) films, $x\sim0.15$ and C$\sim$10 at. %. Again, the films were amorphous and compositionally inhomogeneous, as deduced for the SiO_x and SiC_x films. After annealing to approximately 1050 °C, and as shown in Fig. 7, a feature at 513

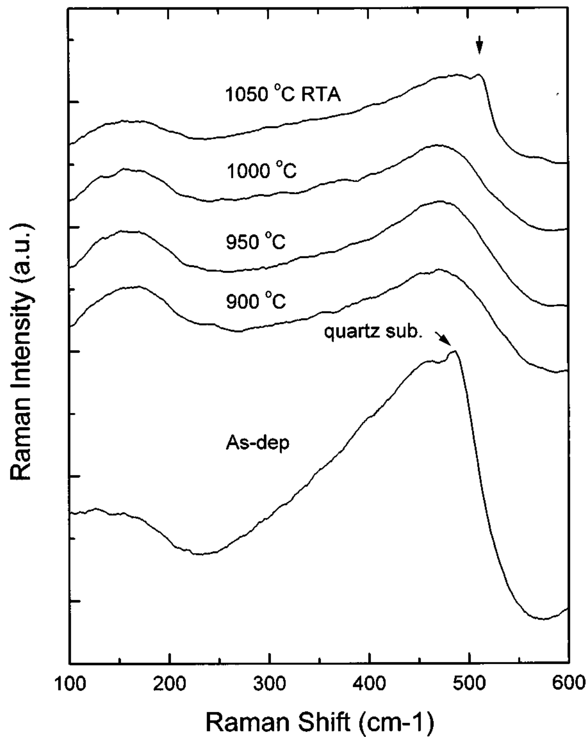

FIG. 7. Raman scattering spectra of $(Si,C)O_x$, $(x\sim0.15$ and C$\sim$10 at. %) thin films before and after annealing.

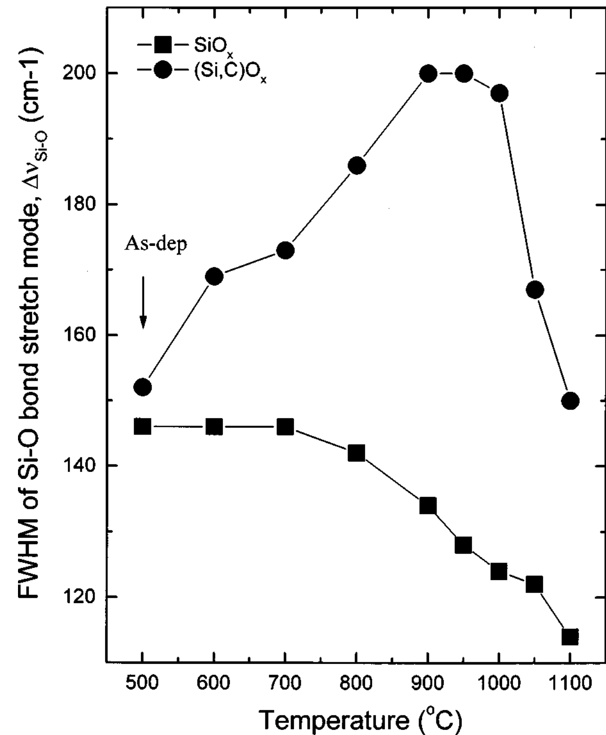

FIG. 9. FWHM, $\Delta\nu$, of the Si–O bond stretch mode as a function of annealing temperature for SiO_x, $(x\sim0.15)$ and $(Si,C)O_x$, $(x\sim0.15$ and C$\sim$10 at. %) thin films.

cm^{-1} represents the formation of nanocrystalline-Si regions. As with the SiC_x films, no other phonon modes of crystalline phases were detected, indicating that crystalline regions of SiC or C were not formed. Note that the peak in the as-deposited spectra at 490 cm^{-1} is due to the quartz substrate.

Figure 8 shows a digitally enhanced, high-resolution TEM image of $(Si,C)O_x$ films, $x\sim0.15$ and C$\sim$10 at. % after annealing to 1050 °C. Consistent with Raman analysis, only randomly oriented crystallites of Si were observed to form throughout the films. The size of the crystallites was approximately 4 nm. The boxes in Fig. 8 outline typical Si crystallites. For annealing temperatures less than 1050 °C, no crystalline products were imaged.

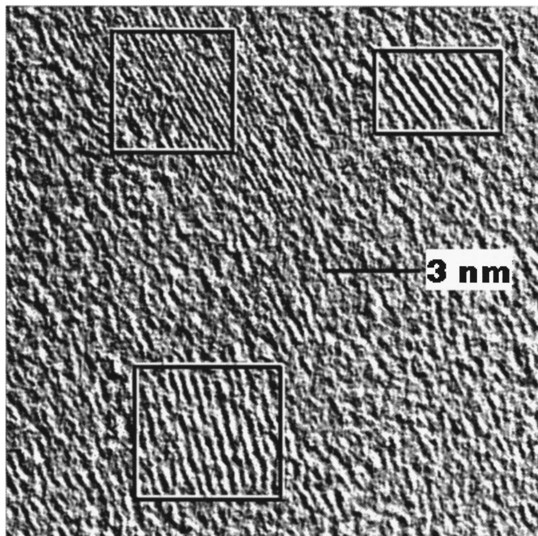

FIG. 8. High-resolution TEM image of a $(Si,C)O_x$, $(x\sim0.15$ and C$\sim$10 at. %) thin film after annealing to 1050 °C.

In summary, the significant bonding and morphology changes that occur between as-deposited films and films annealed at 1050 °C correspond to the formation of stoichiometric, structurally relaxed SiO_2 regions and ordered *a*-SiC regions (from FTIR analysis), and nanocrystalline-Si regions (from Raman and TEM analysis).

IV. DISCUSSION

To further correlate the trends in the data, and also to elucidate the extra feature in the FTIR spectra of the $(Si,C)O_x$ films that has been attributed to Si–O–C arrangements, the full width at half maximum (FWHM), $\Delta\nu$, of the Si–O and Si–C bond stretch modes as a function of annealing temperature has been examined. As the FWHM of these modes decreases, the degree of structural ordering is increased. The FWHM of the Si–O bond stretch mode as a function of annealing temperature for the SiO_x and $(Si,C)O_x$ films is therefore plotted in Fig. 9. The FWHM of the Si–C bond stretching mode for the SiC_x and $(Si,C)O_x$ films as a function of annealing temperature is plotted in Fig. 10. The size of the data points is the standard deviation in these measurements. As shown in Fig. 9, $\Delta\nu$ of the Si–O bond stretch mode for the SiO_x films remains essentially constant upon annealing to 800 °C, and then begins to decrease after 900 °C. This decrease in $\Delta\nu$ after 900 °C annealing corre-

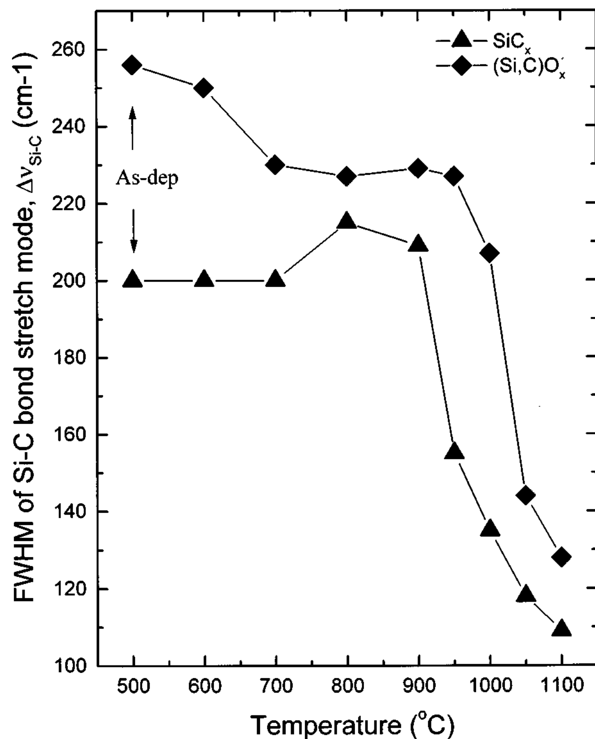

FIG. 10. FWHM, $\Delta\nu$, of the Si–C bond stretch mode as a function of annealing temperature for SiC_x, ($x\sim0.2$) $(SiC)O_x$, ($x\sim0.15$) and C~10 at. %) thin films.

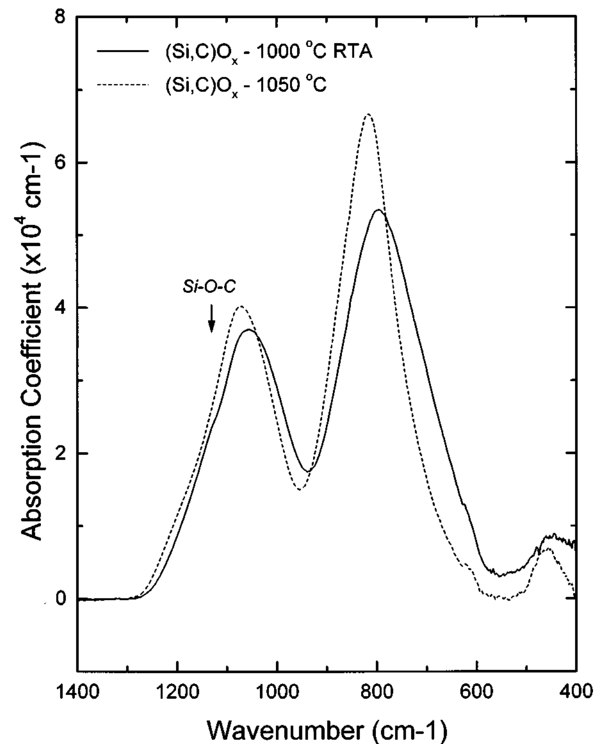

FIG. 11. FTIR absorption spectra of $(Si,C)O_x$,($x\sim0.15$and C~10 at. %) thin films after annealing to 1000 and 1050 °C.

lates (i) with the formation of stoichiometric and structurally relaxed SiO_2 as determined by the shift in the Si–O bond stretching peak position (Fig. 1), and (ii) with the formation of nanocrystalline-Si regions as determined through Raman spectra and TEM (Figs. 2 and 3). In contrast, $\Delta\nu$ of the Si–O bond stretch mode for the $(Si,C)O_x$ films increases significantly upon annealing to 900 °C, remains constant between 900 and 1000 °C, and then drops sharply after annealing to 1050 °C. This trend correlates with results presented above in Figs. 6, 7, and 8. As previously mentioned, a shoulder on the high frequency side of the Si–O stretch mode attributed to Si–O–C bonding was observed to emerge in the spectra of Fig. 6 between annealing temperatures of 900 and 1000 °C, and then *disappear* at 1050 °C. The disappearance of this shoulder after annealing to 1050 °C coincides with (i) a sharp decrease in $\Delta\nu$ of the Si–O stretch mode in Fig. 9, (ii) the formation of stoichiometric and structurally relaxed SiO_2 regions, as determined by the shift in the Si–O bond stretch peak position in Fig. 6, and (iii) the formation of nanocrystalline-Si regions as determined through Raman spectra and TEM in Figs. 7 and 8, respectively.

Figure 10 shows $\Delta\nu$ for the Si–C bond stretching mode in the SiC_x and $(Si,C)O_x$ films as a function of annealing temperature. Again, the trends correlate with previous results. For the SiC_x films, a sharp decrease in $\Delta\nu$ of the Si–C bond stretch mode occurs after annealing to 950 °C, which coincides with (i) the formation of chemically ordered *a*-SiC regions in Fig. 4, and (ii) nanocrystalline-Si regions in Fig. 5. For the $(Si,C)O_x$ films, a sharp decrease in $\Delta\nu$ of the Si–C bond stretching mode does not occur until after annealing to 1050 °C, which coincides with the elimination of Si–O–C bonding groups. This is also consistent with the formation of (i) stoichiometric, thermally relaxed SiO_2 regions and ordered *a*-SiC regions in Fig. 6, and (ii) nanocrystalline-Si regions in Figs. 7 and 8.

Additional quantitative evidence for the elimination of Si–O–C bonding groups in the $(Si,C)O_x$ films upon annealing to 1050 °C is shown in Figs. 11 and 12. Figure 11 shows only the FTIR spectra of $(Si,C)O_x$ films, $x\sim0.15$ and C~10 at. % annealed at 1000 and 1050 °C (compare with Fig. 6). Figure 12 shows the corresponding first derivative spectra in Fig. 11. As shown in Fig. 11, a shoulder is evident at approximately 1125 cm^{-1} after annealing to 1000 °C, and is not present after annealing to 1050 °C. The differentiated spectrum in Fig. 12 after annealing to 1000 °C shows that the derivative decreases abruptly at 1125 cm^{-1} due to the shoulder on the high frequency side of the Si–O bond stretch mode caused by Si–O–C bonding groups. After annealing to 1050 °C, the shoulder is eliminated in Fig. 11 and the corresponding derivative spectrum in Fig. 12 is smooth.

We will now discuss how these results on *bulk* films analyzed in this study correlate with changes in interface bonding and chemistry observed to occur during the thermal oxidation of SiC and subsequent annealing of $SiC–SiO_2$ interfaces. Before doing this we will first consider the SiO_x films. Our results showed that at approximately 900 °C suboxide bonding was eliminated and the films separated into stoichiometric, thermally relaxed SiO_2 regions and nanocrystalline-Si regions. These results are in accordance

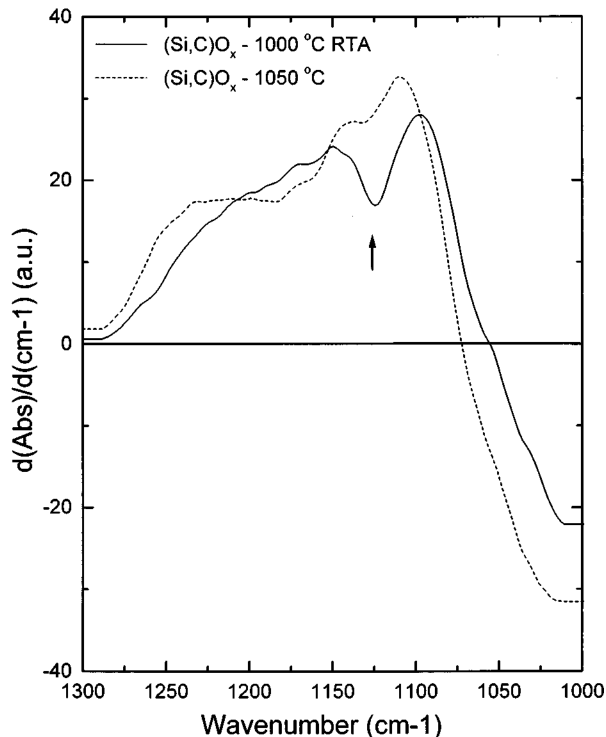

FIG. 12. First derivative FTIR absorption spectra of (Si,C)O_x, ($x \sim 0.15$ and C$\sim$10 at. %) thin films after annealing to 1000 and 1050 °C.

with studies performed directly on Si–SiO_2 interfaces. For example, suboxide bonding at Si–SiO_2 interfaces before and after annealing at 900 °C has been studied by XPS,[7,30,31] AES,[13] TEM,[5] difference x-ray diffraction,[10] and more recently XPS using monochromatic synchrotron radiation.[4] These studies have confirmed the reduction of excess suboxide bonding by annealing in an inert ambient at 900 °C. In addition, the experiments described in Ref. 5 establish that growing an oxide at 900 °C is not equivalent to growth at 900 °C followed by annealing at the same temperature. The apparent saturation of annealing effects in Si–SiO_2 interfaces after 900 °C annealing suggests that the phase separation reaction observed in the deposited SiO_x thin films at 900 °C, i.e., $SiO_x \rightarrow SiO_2 + nc$-Si, also occurs at the crystal interface. However, there are two important differences in the effects that take place at the Si–SiO_2 interface. First, the separation is incomplete at the monolayer level, meaning the annealed Si–SiO_2 interfaces have a residual suboxide bonding on the order of a few monolayers. Second, there is no evidence for the formation of *nc*-Si. The separation reaction results in increased crystallization at the Si–SiO_2 interface, so that in place of the formation of nanocrystallites of Si, Si derived form SiO_x regions is incorporated into the Si substrate.

Now turning to SiC–SiO_2 interfaces, observations based on the occurrence of Si–oxycarbide groups at the interface by XPS,[14] and significant improvements in device performance by an oxidation/annealing sequence[17] in which the oxidation is performed at a temperature in excess of 1025 °C, and the postoxidation anneal at 900 °C are interpreted as follows. Based on the alloy studies presented above which show that oxycarbide bonding is eliminated at approximately 1050 °C, the requirement for a high temperature oxidation is to remove Si–O–C bonding groups that form at the boundary between Si surface atoms and the growing oxide layer. Since device fabrication is usually done on Si faces of 6H or 4H wafers, the annealing step at 900 °C then presumably performs the same function as at Si–SiO_2 interfaces, reducing suboxide bonding in interfacial transitions regions and smoothing the interface.

Finally, the results presented above on the thermochemical stability of silicon oxycarbide thin films deposited via chemical vapor deposition are in accordance with results in the literature on the characterization of silicon oxycarbide glasses prepared from sol–gel precursors.[32,33]

V. CONCLUSIONS

The thermal stability of silicon–oxygen–carbon alloy thin films (Si,C)O_x has been studied by a combination of FTIR spectroscopy, Raman scattering, and high-resolution TEM. Reference films of SiO_x and SiC_x were also prepared and analyzed. Results showed that for the SiO_x films, a structural/chemical transformation takes place at 900 °C in which the films separated into stoichiometric, thermally relaxed SiO_2 and nanocrystalline-Si regions. For the SiC_x films, a structural/chemical transformation takes place at 950 °C in which the films separated into chemically ordered *a*-SiC and nanocrystalline-Si regions. In the (Si,C)O_x system, similar structural/chemical transformations take place at 1050 °C, with the film separating into ordered *a*-SiC regions and stoichiometric, thermally relaxed SiO_2, and nanocrystalline-Si regions. However a very important difference was noted for the (Si,C)O_x films. At temperatures of 900–1000 °C a Si–O–C bonding group was observed to form which in turn has been assumed to inhibit the phase separation process until the Si–O–C bonding group was eliminated at 1050 °C. Important implications of this study towards SiC–SiO_2 interface processing are that oxidation must be performed above 1050 °C to ensure no oxycarbide bonding at the interface and that a 900 °C postoxidation anneal is necessary to reduce suboxide bonding and smooth the interface.

ACKNOWLEDGMENTS

This research has been supported in part by the Office of Naval Research and the Air Force Office of Scientific Research.

[1]F. J. Grunthaner and P. J. Grunthaner, Mater. Sci. Rep. **1**, 69 (1986).
[2]J. Halbritter, J. Mater. Res. **3**, 506 (1988).
[3]T. Hattori, CRC Crit. Rev. Solid State Mater. Sci. **20**, 339 (1995).
[4]J. W. Kiester, J. E. Rowe, J. J. Kododzie, H. Niimi, H.-S. Tao, T. E. Madey, and G. Lucovsky, J. Vac. Sci. Technol. A (these proceedings).
[5]X. Chen and J. M. Gibson, Appl. Phys. Lett. **70**, 1462 (1997).
[6]G. Lucovsky, A. Banerjee, H. Niimi, K. Koh, B. Hinds, C. Meyer, G. Lüpke, and H. Kurz, Appl. Surf. Sci. **117**, 202 (1997).
[7]W. K. Choi, F. W. Poon, F. C. Loh, and K. L. Tan, J. Appl. Phys. **81**, 7386 (1997).
[8]K. Ishikawa, Y. Uchiyama, H. Ogawa, and S. Fujimura, Appl. Surf. Sci. **117**, 212 (1997).

[9]N. Yasuda, S. Takagi, and A. Toriumi, Appl. Surf. Sci. **117**, 216 (1997).
[10]N. Awaji, S. Ohkubo, T. Nakanishi, K. Takasaki, and S. Komiya, Appl. Surf. Sci. **117**, 221 (1997).
[11]A. Toriumi, H. Satake, N. Yasuda, and T. Tanamoto, Appl. Surf. Sci. **117**, 230 (1997).
[12]T. Sakoda, M. Matsumura, and Y. Nishioka, Appl. Surf. Sci. **117**, 241 (1997).
[13]G. Lucovsky, A. Banerjee, B. Hinds, B. Claflin, K. Koh, and H. Yang, J. Vac. Sci. Technol. B **15**, 1074 (1997).
[14]B. Hornetz, H-J. Michel, and J. Halbritter, J. Mater. Res. **9**, 3088 (1994).
[15]M. I. Chaudrhy, J. Mater. Res. **4**, 404 (1989).
[16]C. Önneby and C. G. Pantano, J. Vac. Sci. Technol. A **15**, 1597 (1997).
[17]L. Lipkin and J. W. Palmour, J. Electron. Mater. **25**, 909 (1996).
[18]K. I. Luthra, J. Am. Ceram. Soc. **74**, 1095 (1991).
[19]D. V. Tsu, G. Lucovsky, and B. N. Davidson, Phys. Rev. B **40**, 1795 (1989).
[20]B. J. Hinds, F. Wang, D. M. Wolfe, C. L. Hinkle, and G. Lucovsky, J. Non-Cryst. Solids **227**, 507 (1998).
[21]G. Lucovsky, J. Non-Cryst. Solids **227**, 1 (1998).
[22]G. Lucovsky, D. V. Tsu, R. A. Rudder, and R. J. Markunas, in *Thin film Processes II*, edited by J. L. Vossen and W. Kern (Academic, San Diego, 1991), pp. 565–619.
[23]D. M. Wolfe, F. Wang, B. J. Hinds, and G. Lucovsky, Mater. Res. Soc. Symp. Proc. **483**, 203 (1998).
[24]G. Lucovsky, J. Yang, S. S. Chao, J. E. Tyler, and W. Czubatyj, Phys. Rev. B **28**, 3224 (1983).
[25]G. Socrates, *Infrared Characteristic Group Frequencies*, 2nd ed. (Wiley, Chichester, 1994), Chap. 18.
[26]H. Reubel, B. Schroeder, W. Fuhs, J. Krauskopf, T. Rupp, and K. Bethge, Phys. Status Solidi B **139**, 131 (1987).
[27]D. W. Feldman, J. H. Parker, Jr., W.J. Choyke, and L. Patrick, Phys. Rev. **173**, 787 (1968).
[28]L. J. Bellamy, *The Infrared Spectra of Complex Molecules* (Chapman and Hall, London, 1975), Chap. 20.
[29]A. L. Smith, *The Analytical Chemistry of Silicones* (Wiley, New York, 1991), p. 336.
[30]G. Hollinger and F. J. Himpsel, Appl. Phys. Lett. **44**, 93 (1984).
[31]P. J. Grunthaner, M. H. Hecht, F. J. Grunthaner, and N. M. Johnson, J. Appl. Phys. **61**, 629 (1987).
[32]H. Zhang and C. G. Pantano, J. Am. Ceram. Soc. **73**, 958 (1990).
[33]G. D. Sorarù, G. D'Andrea, R. Campostrini, F. Babonneau, and G. Mariotto, J. Am. Ceram. Soc. **78**, 379 (1995).